# 1 Mathematical model

We use a computational hybrid model based on that presented in McLennan et al. (2012, 2015a,b, 2017). The model is a two-dimensional approximation of the system and consists of a discrete, off-lattice model for the dynamics of neural crest cells, coupled to a continuum, reaction-diffusion model for the dynamics of the chemoattractant VEGF. We implement the model using Aboria (Robinson and Bruna, 2017, https://martinjrobins.github.io/Aboria/), a C++ library for particle-based numerical methods.

## 1.1 Dynamics of cells

We describe briefly how we incorporate the dynamics of cells. We assume that there are two types of cells, namely "leaders" and "followers". Leaders undertake a fixed-jump-length biased random walk up a cell-induced gradient of chemoattractant. To model cells extending filopodia to sense the concentration of chemoattractant at their tips we sample the chemoattractant concentration at a certain number of points a fixed distance away from the center of a cell in randomly chosen directions. The cells move in the direction of the highest concentration sensed, provided it is sufficiently higher (regulated by the sensing accuracy parameter $\mu$) than the chemoattractant concentration at the position of the center of the cell. If this is not the case, then we move the cell in a random direction. On the other hand, followers are either in chains or they move randomly. A chain consists of a group of followers that are close to each other, with at least one of them close to a leader. All the followers in a chain move in the same direction as the leader that is at the front of that chain. If a follower is able to follow more than one cell, i.e. it could join multiple chains, it randomly chooses one to join.

We include phenotype switching based on the position of a cell within the migratory stream. We make a simplification from the previous model by McLennan et al. (2015a) and assume that the phenotype is determined based on cell position rather than VEGF concentration. This simplification is consistent with the experimental observation that gene expression profiles depend on the position of a cell within a migratory stream, with a small number of leaders at the very front of the stream where the concentration of VEGF is the highest (McLennan et al., 2015a). A constant number of leaders is a reasonable assumption in our model because we do not model the system with experimental perturbations in VEGF distribution that have been shown to alter the number of leaders (McLennan et al., 2015b).

## 1.2 Model assumptions

We now list the key assumptions used in the model. Firstly, we use a fixed time-step model ($\Delta t = 1$min) during which a cell senses its environment and updates its position. Secondly, we model volume exclusion by considering cells as hard-discs that are not allowed to overlap (in reality, cells will deform when they come into contact with each other, so this is a model simplification). If a cell cannot make a

movement due to volume exclusion, i.e. the target destination is occupied by other cells, then it remains in the same position. Thirdly, we assume that the entire cell body has to be inside the rectangular domain. We allow a cell to extend filopodia outside the domain but, in our model, this never leads to a movement in that direction. If all the filopodia of a cell are extended outside the domain, and the random direction sampled leads to a movement outside the domain, then the cell does not move. These rules provide the boundary conditions for cells everywhere apart from the neural tube ($x$ = 0) where there is an influx of cells. There is an attempt to insert a new cell at every time step with its center at a random position along the $y$-axis and $x =$ cell radius (that is, the cell is placed fully inside the domain).

## 1.3 Domain

We use a rectangular two-dimensional domain $(x, y) \in [0, L_x(t)] \times [0, L_y]$ as a simplification of the narrow (in height) curved three-dimensional migratory path (Figure 1). Initially, we consider uniform in space domain growth in the $x$-direction, then we split the domain into two parts, which we call Part 1 and Part 2, respectively (Figure 1), that grow at different rates. Based on experimental results, we assume that for $0 < t < 18$hrs Part 1 elongates twice as fast as Part 2 and for $18 \leq t < 24$hrs Part 2 elongates twice as fast as Part 1 (Figure 3). We assume that growth is exponential. We use experimental data on the initial and final lengths of the domain to estimate growth parameters. To find the two different growth rates we solve equation (1)

$$P_1 exp(A_1 \alpha t_{final}) + P_2 exp(A_2 \alpha t_{final}) = L_{final}, \tag{1}$$

for $\alpha$, where $P_1$ is the initial length of Part 1, $P_2$ is the initial length of Part 2, $L_{final}$ is the final total length of the domain and factors $A_1$ and $A_2$ determine which part of the domain grows faster, for example, if Part 1 grows twice as fast as Part 2, then $A_1 = 2$ and $A_2 = 1$. The growth rates are $A_1\alpha$ and $A_2\alpha$ for Part 1 and Part 2, respectively.

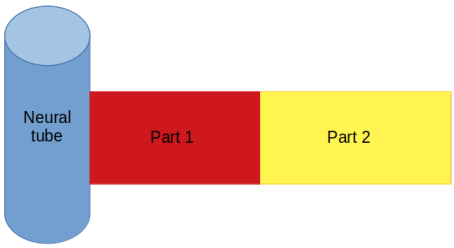


**Figure 1:** Domain divided into two parts, Part 1 and Part 2. We will consider different percentage of Part 1 and Part 2, see figure below.

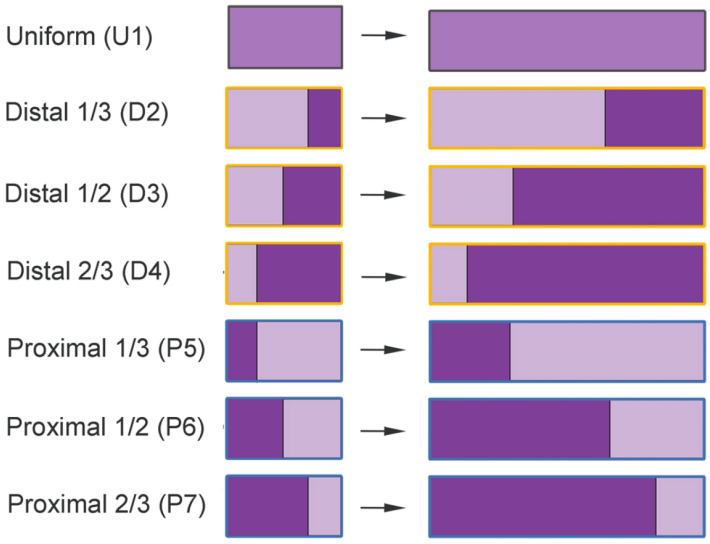


**Figure 2**

**Figure 3:** Growth profiles: different parts of the domain grow. Darker part grows twice as fast as the lighter part. U1 represents uniform growth. D2-5 represent distal part of the domain growing twice faster than the proximal part. P5-7 represent proximal part of the domain growing twice faster than the distal part. The total length of the domain increases to the same value in all cases.

## 1.4 Chemoattractant dynamics

We use a reaction-diffusion equation to model the dynamics of the chemoattractant VEGF but, whereas the model by McLennan et al. (2012, 2015a,b, 2017) was restricted to uniform domain growth, our model can incorporate any domain growth function (Crampin et al., 1999, 2002). We scale the concentration of VEGF, $c(x, y, t)$, to $c \in [0, 1]$ and define the equation on the growing domain with $x \in [0, L_x(t)]$ and $y \in [0, L_y]$ (parameter values in Table 1):

$$\frac{\partial c}{\partial t} + \underbrace{\frac{\partial (ac)}{\partial x}}_{(i)} = \underbrace{D\left(\frac{\partial^2 c}{\partial x^2} + \frac{\partial^2 c}{\partial y^2}\right)}_{(ii)} \underbrace{- c \sum_{i=1}^{N(t)} \frac{\lambda}{2\pi R^2} exp\left[-\frac{(x - x_i)^2 + (y - y_i)^2}{2R^2}\right]}_{(iii)} + \underbrace{\kappa c(1 - c)}_{(iv)}, \tag{2}$$

where $D$ is the diffusion coefficient of the chemoattractant, $R$ is the cell radius, $\lambda$ is the internalization rate, $\kappa$ is the production rate of the chemoattractant, $a$ is the flow due to domain growth, $N(t)$ is the number of cells at time $t$ and $(x_i, y_i)$, $i = 1, \ldots, N(t)$ is the position of the center of cell $i$. We assume zero flux boundary conditions and initial conditions $c(x, y, 0) \equiv 1$. We assume a uniform initial condition based on the observations that prior to NC migration VEGF is spatially uniform in the tissue up to the entrance to ba2 (McLennan et al., 2010).

We briefly explain the reasoning behind the terms of equation (2). Term $(i)$ corresponds to the effect of domain growth. It consists of an advection term, $a \times \partial c/\partial x$, corresponding to elemental areas moving with the flow due to local growth, and a dilution term, $c \times \partial a/\partial x$, due to local area change. Term $(ii)$

corresponds to diffusion of chemoattractant with diffusion coefficient $D$. Term $(iii)$ is the internalization of chemoattractant by cells. We use a simple Gaussian kernel because it takes into account the size of cells, and we assume that the cells consume or degrade the chemical with a continually decreasing intensity moving away from the cell center. Term $(iv)$ is the production of chemoattractant. We assume logistic production, however, since the production rate, $\kappa$, is relatively small in comparison with the internalization rate, $\lambda$ (see McLennan et al., 2010), the dynamics do not change significantly when other forms of production, such as linear or constant, are considered. Assuming that the flow can be specified using a growth function $\Gamma$, the Lagrangian description is

$$x = \Gamma(X, t), \qquad x \in [0, L_x(t)], \tag{3}$$

where $X \in [0, X_0]$ is an initial position marker with $X_0 = L_x(0)$, and $\Gamma(X, 0) = X$. The local flow is determined by

$$a(x, t) = \frac{\partial x}{\partial t} = \frac{\partial \Gamma}{\partial t}. \tag{4}$$

The term that specifies growth is $\partial a/\partial x$. Let us assume that it can be expressed as

$$\frac{\partial a}{\partial x} = S(X, t), \tag{5}$$

where $S(X, t)$ is the strain rate. Our Lagrangian form gives the description of the flow

$$a(x, t) = a(\Gamma(X, t), t) = \frac{\partial \Gamma}{\partial t}. \tag{6}$$

Combining equations (5) and (6) gives

$$\frac{\partial^2 \Gamma}{\partial t \partial X} = \frac{\partial a}{\partial X} = S(X, t)\frac{\partial \Gamma}{\partial X} \tag{7}$$

with initial condition $\Gamma(X, 0) = X$ and boundary conditions $\Gamma(0, t) = 0$ and $\Gamma(1, t) = L_x(t)$. The solution to equation (7) is

$$\Gamma(X, t) = \int_0^X \left[ exp \int_0^t S(z, \tau) d\tau \right] dz \tag{8}$$

It sometimes can be difficult to evaluate $\Gamma(X, t)$ for a given strain rate $S(X, t)$. Therefore, it is useful to switch to Lagrangian coordinates. Writing variables as functions of initial position $X$ and time $t$ (setting $C(X, t) = c(x, t)$) in equation (2) and using equations (3)-(7) gives

$$\frac{\partial C}{\partial t} + CS(X, t) = D\left(\frac{1}{\Gamma_X}\frac{\partial}{\partial X}\left(\frac{1}{\Gamma_X}\frac{\partial C}{\partial X}\right) + \frac{\partial^2 C}{\partial y^2}\right) + f(C). \tag{9}$$

where

$$f(C) = \kappa C(1 - C) - C\sum_{i=1}^{N(t)} \frac{\lambda}{2\pi R^2} exp\left[-\frac{(\Gamma(X) - x_i)^2 + (y - y_i)^2}{2R^2}\right]. \tag{10}$$

Equation (9) only requires us to determine $\Gamma_X$, which can be done using equation (7). We use this form because we want our framework to be flexible enough to incorporate for any strain rate $S(X, t)$, which we estimate from experimental data. We solve equation (9) using an explicit finite difference method (second-order midpoint rule in space, and forward Euler in time) with $\Delta x = 1\mu$m, $\Delta y = 1\mu$m and $\Delta t_c = 12$s. Note that a time step of 12s is equivalent to the discrete simulation time step for the

cell motility model (see Table 1). These choices are sufficient for the algorithm to converge and resolve accurately the gradient of VEGF. We validate our solution using the manufactured solution method (Roache, 2002), verify convergence by reducing space and time steps by a factor of ten and tracking the average relative error (which is less than $10^{-3}$), and ensure stability using the von Neumann stability condition.

## 1.5 Pseudocode

We provide a pseudocode that explains in detail how we numerically simulate the model. The text in blue corresponds to the steps that are only applicable for the model with a tunneling mechanism included. The full code is available at https://github.com/rginiunaite/NC-cells-non-uniform-domain-growth. Note that a user first needs to install the Aboria library (https://martinjrobins.github.io/Aboria/).

---

**Main steps**

1. Initialise model parameters and insert $N_{leader}$ leader cells at $x = R$ and equal distance apart in the $y$-direction, set $t = 0$.
2. Choose a random position in $y$ with $x = R$. If there is no overlap with other cells, then insert a new follower cell at this position.
3. Solve chemoattractant profile.
4. Grow domain (update $\Gamma(X, t)$)) and update cell positions due to advection by the growth.
5. Move cells.
6. Implement any phenotype switching.

**Internal steps**

*cell advection due to domain growth*

1. **for** $i$ = 1 to number of cells **do**
2. for a cell with its center at $(x_i, y_i)$, find $Z$, a point on the space grid in the $x$-direction, such that $\Gamma(Z, t - \Delta t) < x_i < \Gamma(Z + \Delta x, t - \Delta t)$
3. update the cell position to $(x_i + \Gamma(Z, t) - \Gamma(Z, t - \Delta t), y_i))$
4. **end for**

*move cells* (Note that if a cell cannot move due to volume exclusion then the attempted movement is aborted)

1. **for** $i$ = 1 to number of cells **do**
2. pick a cell at random without replacement
3. **if** the cell is a leader, **then**

4. pick $n_{filo}$ random directions and measure chemoattractant concentration in those random direction(s) at distance $l_{filo}$ away from the center of the cell, pick the highest concentration and set it to $c_{new}$, measure chemoattractant concentration at the center of the cell and set it to $c_{old}$
5. **if** $\frac{c_{new}-c_{old}}{\sqrt{c_{old}}} \geq \mu$ (sensing accuracy), **then**
6. move in chosen direction a distance $\Delta t \times \nu$
7. **end if**
8. **else**
9. move in random direction a distance $\Delta t \times \nu$
10. **end if**
11. **end if**
12. **end if**
13. **else** (the cell is a follower)
14. **if** the cell is in a chain, **then**
15. move a distance $\Delta t \times ratio \times \nu$ in the same direction as the leader at the front of the chain
16. **if** the cell is further away than $l_{filo}^{max}$ from the cell which it was following, **then**
17. detach it, and all the cells that were following it, from the chain
18. **end if**
19. **end if**
20. **if** the cell is not in a chain, **then**
21. **if** there is a leader or a follower in a chain less than $l_{filo}$ distance away, **then** join that chain (if there are multiple possibilities, pick one randomly) and move a distance $\Delta t \times ratio \times \nu$ in the same direction as the cell ahead in the chain
22. **end if**
23. **else** move a distance $\Delta t \times ratio \times \nu$ in a random direction
24. **end if**
25. **end for**

*phenotype switching*

1. **for** $i$ = 1 to number of cells **do**
2. **if** a cell is a follower **then**
3. **if** the cell is further ahead by $\epsilon$ in the $x$-direction than one of the leaders and it is sufficiently close to that leader, **then** swap their phenotype **end if**
4. **end if**
5. **end for**

---

| | **Description** | **Value** | Reference |
|---|---|---|---|
| $N_{leader}$ | number of leaders | 5 | comments |
| $n_{filo}$ | directions sampled per time step, filopdia number | 1-3 | results section |
| $\Delta t$ | simulation time step, s | 12 | n/a |
| $R$ | cell radius (nuclear), μm | 7.5 | McLennan and Kulesa (2010) |
| $\nu$ | input leader cell speed, μm/min | 0.7 | comments |
| $ratio$ | ratio of follower to leader speed | 1.3 | comments |
| $L_y$ | width of migratory domain, μm | 120 | experimental data |
| $L_x(t)$ | length of migratory domain, μm | 342 to 1100 | experimental data |
| $l_{filo}$ | sensing radius, μm | 27.5 | comments |
| $\sigma$ | maximum cell separation before contact is lost, μm | 45 | comments |
| $\mu$ | sensing accuracy | 0.05 | comments |
| $D$ | diffusion coefficient of chemoattractant, $\mu m^2/min$ | 10.0 | comments |
| $\kappa$ | production rate of chemoattractant, /min | 5.0 | comments |
| $\lambda$ | chemoattractant internalization rate, $\mu m^2/min$ | 5.0 | comments |
| $\epsilon$ | distance a follower has to be ahead of a leader to swap phenotypes, μm | 10 | comments |

**Table 1:** Model parameters used in the simulations provided in the results section.

## 1.6 Ablation experiments

For physical ablation of cells, we delayed the influx of cells by two hours and then changed the attempt to insert new cells from every step to every ten steps (step two in the Pseudocode).

For chemical inhibition of domain growth, we specified new final domain length based on experimental data and obtained new model parameters. Domain growth was reduced uniformly.

## 1.7 Model parameters

We choose most of our parameters based on those from McLennan et al. (2015a,b, 2017). Table 1 contains the values we used for the computational results of this paper.

**Comments**

- We use a fixed-jump-length process where the length of the jump is $\Delta t \times \nu$ for leaders and $\Delta t \times ratio \times \nu$ for followers.

- $N_{leader}$ - number of leaders. We choose a fixed number of five leaders because we find that this is the smallest number of cells that can guide the rest of the population successfully (either by contact or tunnels, results not shown). A higher number of leader cells could be chosen provided that we adjust the internalization rate, the sensing accuracy and the diffusion coefficient to avoid some leaders getting stuck due to the lack of a gradient of chemoattractant.

- $ratio$ - ratio of follower to leader speed. Kulesa et al. (2008) demonstrated that the speed of the followers is higher than that of the leaders. We chose a $ratio$ value sufficiently high to ensure that the stream does not break in the control case.

- $l_{filo}$ - sensing radius. We use the value calculated by McLennan et al. (2015) as the sum of the cell radius and the mean filopodial length.

- $l_{filo}^{max}$ - maximum cell separation before contact is lost. We use the value calculated by McLennan et al. (2015), obtained from half of the maximum cell size including filopodium.

- $\mu$ - sensing accuracy. We use the same argument for the accuracy with which the cells can sense a chemical gradient as McLennan et al. (2012, 2015, 2015, 2017). They base their work on the biophysical limit for sensing accuracy derived by Berg and Purcell (1977). Briefly, they assume that fluctuations in molecule number are proportional to $\sqrt{N}$, where $N$ is molecule number. Since we use a continuum variable for the chemoattractant, fluctuations can be expressed as $\sqrt{Ac}$ where $A$ is some area of interest, and $c$ is the average concentration in that area. The inaccuracy of concentration measurements is inversely proportional to fluctuations, which gives

$$\frac{\Delta c}{c} \approx \frac{1}{\sqrt{N}} = \frac{1}{\sqrt{Ac}}. \tag{11}$$

  Rearranging gives

$$\frac{\Delta c}{\sqrt{c}} \approx \mu, \tag{12}$$

  where we define $\mu$ as the sensing accuracy, and $\Delta c = c_{new} - c_{old}$. $\Delta c/\sqrt{c_{old}}$ has to be greater than or equal to $\mu$ for the cell to respond. We choose $\mu$ sufficiently high to ensure that movement does not occur in response to very small changes in VEGF concentration. The results are robust if we change this parameter together with the internalization rate $\lambda$.

- $D$ - diffusion coefficient of chemoattractant. The exact value of the diffusion coefficient is unknown for the system. We use a relatively small value because it has been shown that only around $1\%$ of VEGF freely diffuses, whilst the rest binds to the ECM (Mac Gabhann et al. 2006). The results are robust to changes in this parameter because it only affects the sharpness of the gradient of VEGF. Changes in the internalization rate, $\lambda$, and the sensing accuracy, $\mu$, also influence the choice of the diffusion coefficient.

- $\kappa$ - production rate of chemoattractant. The exact VEGF production rate in the tissue is unknown, but since experimental results show that there is almost no VEGF produced where the cells have already internalized it (McLennan et al. 2010), we assume that the production rate is small.

- $\lambda$ - chemoattractant internalization rate. As the internalization rate is also unknown, we choose this parameter based on the distance traveled by cells in 24h. The results are robust to simultaneous changes in the sensing accuracy, $\mu$, and the internalization rate, $\lambda$, therefore we adapted the internalization rate to our chosen sensing accuracy, $\mu$.
- $\epsilon$ - distance a follower has to be ahead of a leader to swap phenotypes. As discussed in Section 1.4, we use a simplified version of the switching mechanism based on the position in the stream. We assume that a follower has to be $\epsilon = 10\mu$m ahead of a leader for their phenotypes to swap. The results are robust to changes in this parameter because we have a fixed number of leaders.
- We measure effective NC cell speed by recording cell positions every seven minutes and measuring the change in cell position in those seven minutes.

# References


Berg, H. C. and Purcell, E. M. (1977). Physics of chemoreception. *Biophysical journal*, 20(2):193–219.

Crampin, E. J., Gaffney, E. A., and Maini, P. K. (1999). Reaction and diffusion on growing domains: scenarios for robust pattern formation. *Bulletin of Mathematical Biology*, 61(6):1093–1120.

Crampin, E. J., Hackborn, W. W., and Maini, P. K. (2002). Pattern formation in reaction-diffusion models with nonuniform domain growth. *Bulletin of Mathematical Biology*, 64(4):747–769.

Kulesa, P. M., Teddy, J. M., Stark, D. A., Smith, S. E., and McLennan, R. (2008). Neural crest invasion is a spatially-ordered progression into the head with higher cell proliferation at the migratory front as revealed by the photoactivatable protein, kikgr. *Developmental Biology*, 316(2):275–287.

McLennan, R., Bailey, C. M., Schumacher, L. J., Teddy, J. M., Morrison, J. A., Kasemeier-Kulesa, J. C., Wolfe, L. A., Gogol, M. M., Baker, R. E., Maini, P. K., et al. (2017). DAN (NBL1) promotes collective neural crest migration by restraining uncontrolled invasion. *Journal of Cell Biology*, 216(10):3339–3354.

McLennan, R., Dyson, L., Prather, K. W., Morrison, J. A., Baker, R. E., Maini, P. K., and Kulesa, P. M. (2012). Multiscale mechanisms of cell migration during development: theory and experiment. *Development*, 139(16):2935–2944.

McLennan, R., Schumacher, L. J., Morrison, J. A., Teddy, J. M., Ridenour, D. A., Box, A. C., Semerad, C. L., Li, H., McDowell, W., Kay, D., et al. (2015a). Neural crest migration is driven by a few trailblazer cells with a unique molecular signature narrowly confined to the invasive front. *Development*, 142 11:2014–25.

McLennan, R., Schumacher, L. J., Morrison, J. A., Teddy, J. M., Ridenour, D. A., Box, A. C., Semerad, C. L., Li, H., McDowell, W., Kay, D., Maini, P. K., Baker, R. E., and Kulesa, P. M. (2015b). VEGF signals

induce trailblazer cell identity that drives neural crest migration. *Developmental Biology*, 407(1):12–25.

McLennan, R., Teddy, J. M., Kasemeier-Kulesa, J. C., Romine, M. H., and Kulesa, P. M. (2010). Vascular endothelial growth factor (VEGF) regulates cranial neural crest migration in vivo. *Developmental Biology*, 339(1):114–125.

Roache, P. J. (2002). Code verification by the method of manufactured solutions. *Journal of Fluids Engineering*, 124(1):4–10.

Robinson, M. and Bruna, M. (2017). Particle-based and meshless methods with Aboria. *SoftwareX*, 6:172 – 178.